Novel Modeling and Damping Technique for Hybrid Stepper Motor

Kenneth Wang-Hay Tsui, Norbert Chow Cheung, *Senior Member, IEEE*, and Kadett Chi-Wah Yuen

***Abstract*—It is well known that commercial hybrid stepper system has one or more low-speed resonant points. However, this characteristic cannot be accurately modeled without high-order equations or complicated measurement of motor parameters. In this paper, a novel approach is proposed to model the behavior of a commercial 1.8° hybrid stepper motor accurately and efficiently. Also, model-based damping algorithms for both open-loop control and servo control are proposed. Simulation and experimental results show that the proposed algorithms can effectively eliminate low-speed resonance and vibration of the stepper system. The algorithms are efficient enough to be implemented on commercial DSP-based controllers without sacrificing motion control performance.**

***Index Terms*—Damping, modeling, resonances, Stepper motors.**

I. Introduction

THE stepper motor system has several significant advantages. No feedback is normally required for either position control or speed control. Positional error is nonaccumulative. In addition, stepper motors are compatible with modern digital equipment. For these reasons, various types and classes of stepping motor have been used in computer peripheral, automated machinery, and similar system [1]. The cost of the stepper system is significantly lower than that of the servo system. It is mainly because of the removal of high cost of the position feedback device and complicated feedback control. Moreover, it does not require tuning of feedback control which needs extra expertise and effort. Simple hardware and control configuration also improve system reliability.

One of the most unfavorable features of stepper motor is mechanical resonance, particularly at low speed (typically below 300 r/min). The problem is less significant at high speed because the vibration exceeds the bandwidth of most mechanical system. Resonance prevents stepper motor to run steadily at certain speeds and reduce the motor's usable torque. This prevents stepper motor to be used on application that requires smooth low-speed motion.

For a stepper system, the frequency of oscillation can be predicted for any motor/load combination from the static torque/rotor position characteristic, provided that the system is lightly damped. The natural frequency of rotor oscillation about the equilibrium position is [2]

$$f_n = \frac{1}{2\pi}\sqrt{\frac{T'}{J}} \tag{1}$$

where

T' stiffness of the τ/θ characteristic;
J rotor inertia (in kilogram square meters);
f_n natural frequency (in hertz).

Possible excitation of vibration includes discrete stepping motion, detent torque of permanent magnet, pole-to-pole variation, etc. With the popularity of microstep drive, stepping ripple has been greatly minimized. However, even if the motor is driven with perfect sinusoidal current waveform, vibration and resonance still exist due to motor characteristics.

In the past, much effort has been spent on improving the performance of stepper system in various ways. Brown and Srinivas [3] attempted to use resistance and capacitance to increase electric damping at particular frequency. It showed some advantages at the expense of system efficiency and circuit complexity. Schweid *et al.* [4] developed a nonlinear analog position controller to regulate the velocity of hybrid stepper system. The proposed velocity damping showed some effects at low speed, and the integral control could decouple the steady-state position response with the external torque.

Zribi and Chiasson [5] demonstrated that stepper system could be fast and accurate with exact feedback-linearized position control. They also showed that the linearization was, in fact, the well-known direct-quadrature (DQ) transformation if the detent torque was not considered. Crnosija *et al.* [6] had implemented the optimal algorithm for closed-loop control. Chen *et al.* [7] improved profile tracking performance by using a model-based feedback controller with a least-squares-based identification procedure. Furthermore, they had exploited learning control for precision control at low speed [8]. Betin *et al.* [9] had applied fuzzy logic principle on closed-loop speed control of stepping motor. Hwang *et al.* [10] improved the position accuracy through a closed-loop control scheme. However, the performance of the mentioned algorithms was highly dependent on the resolution of the position feedback device. The feedback device also increased the system cost and was not commercially favorable.

Goodnick [11] reported the satisfactory result of electronic damping based on the estimated velocity, which was found by integrating the estimated motor torque. However, its performance would be limited by the noisy torque estimation. Yang and Kuo [12] reported the effective damping algorithm

Manuscript received April 18, 2007; revised April 9, 2008. First published November 7, 2008; current version published December 30, 2008. This work was supported in part by ASM Assembly Automation Ltd. and in part by The Hong Kong Polytechnic University through the Teaching Company Scheme under Project ZW82.

K. W.-H. Tsui and K. C.-W. Yuen are with ASM Assembly Automation Ltd., Hong Kong (e-mail: whtsui@asmpt.com).

N. C. Cheung is with the Department of Electrical Engineering, The Hong Kong Polytechnic University, Kowloon, Hong Kong (e-mail: norbert.cheung@polyu.edu.hk).

Digital Object Identifier 10.1109/TIE.2008.2008791

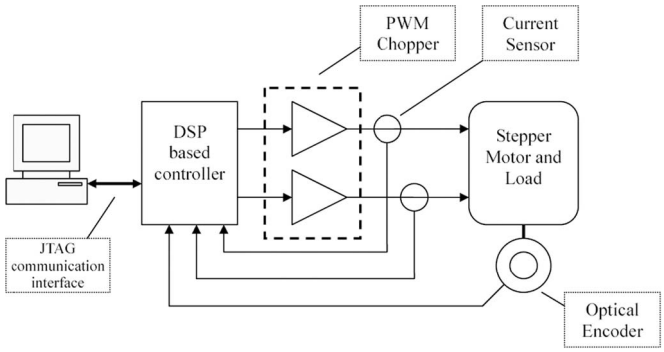

Fig. 1. Block diagram of the stepper system for investigation.

based on a PLL position and velocity observer. Unfortunately, errors in position estimation would accumulate with time due to the use of integrator. The sensorless-based algorithm generally involves large amount of computation. Stepper motor typically has high pole count. Current at 1 kHz is required to drive a 50-pole-pair 1.8° motor at 1200 r/min. The computation power of commercial processor limits the update rate to a few kilohertz, and the system works only at low speed.

As introduced by Bose [13], artificial neural network (ANN) techniques have recently had an impact on power electronics and motor drives. Sanchez *et al.* [14] proposed a sliding-mode control law based on the ANN identifier for trajectory tracking. Rubaai *et al.* [15]–[17] had exploited ANN-based techniques for high-performance stepper motor drives. However, the developing ANN-based techniques are often facing challenges on convergence and overtraining.

Further work must be done to develop an effective and efficient electronic damping algorithm for hybrid stepper motor. In this paper, a new torque expression is proposed to model the vibration and resonance of commercial hybrid stepper motor, particularly at low and medium speeds. This is done without using high-order equations and complicated identification procedures. Model-based damping algorithms are proposed for both open-loop and servo modes. Both simulation and experimental results show that the proposed algorithms can obtain vibration- and resonance-free motion from low to medium speed. The algorithm is efficient enough to update at 40 kHz on commercial DSP which can provide the performance even for demanding applications.

II. Modeling of Stepper Motor

A. System for Investigation

The block diagram of the hardware platform for our investigation is shown in Fig. 1. The controller is based on TI 2810 DSP which handles all motion control, profile generation, and current control. The controller is programmed and commanded by a standard PC through the JTAG interface. It outputs 20-kHz center-aligned pulsewidth modulation (PWM) signals to control a three-phase chopper power drive, which generates the driving current for the motor. Current feedback for current control is provided by a high-bandwidth Hall-effect current sensor whose bandwidth is larger than 100 kHz.

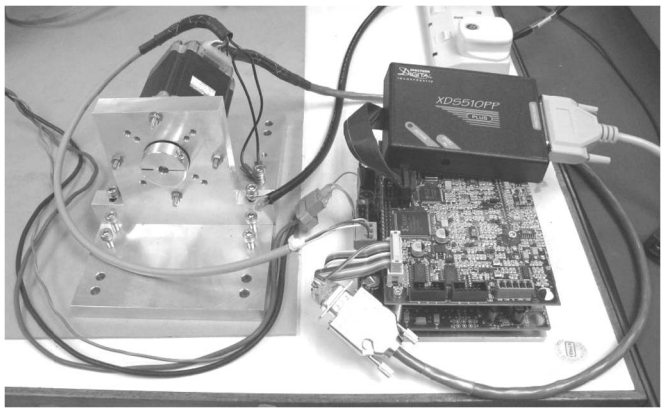

Fig. 2. Hardware platform for investigation.

A commercial 1.8° hybrid stepper motor is chosen for our studies. It is a 50-pole-pair motor with coil resistance of 0.9 Ω, coil inductance of 2.2 mH, rotor inertia of 0.36×10^{-4} kg · m^2, rated current of 3 A, holding torque of 1.27 N · m, and force constant (K_m) of 0.3 N · m/A. The motor is optimized for microstepping control. An optical encoder (1000 lines, 4000 pulses/rev) is attached to the motor for performance monitoring. It is also used as position feedback for the position loop in servo mode. A photograph of the hardware platform is shown in Fig. 2.

To generate center-aligned PWM, DSP general-purpose timer 1 is set to count upward and downward continuously at 50-μs period, as shown in Fig. 3. The timer also generates an underflow interrupt when it hits zero which triggers the ADC to start converting the current feedback signal. At the same time, the interrupt service subroutine (ISR) is started which handles all real-time functions including motion profile generation, position control, damping algorithm, current control, and data logging. The PWM duty cycle calculated during the ISR is updated into the register of PWM generator when timer 1 counter hit the peak. Assuming that PWM toggles in the middle of the cycle, the best and worst case delays for the current controller to respond are 37.5 and 82.5 μs, respectively. ADC conversion takes about 5 μs, and the ISR takes no more than 24 μs in our implementation. No code optimization is done at this stage. The ISR time mentioned is thus a very conservative estimation.

B. Proposed Stepper Model

The simplified stepper model is used most of the time for efficiency. The simplified stepper electrical dynamics and torque expression are shown as follows [18]:

$$\frac{di_{a\_\mathrm{fb}}}{dt} = -\frac{R}{L_o} i_{a\_\mathrm{fb}} + \frac{K_m}{L_o}\omega_{\mathrm{fb}} \sin(N_r\theta_{\mathrm{fb}}) + \frac{v_{A+} - v_{A-}}{L_o} \tag{2}$$

$$\frac{di_{b\_\mathrm{fb}}}{dt} = -\frac{R}{L_o} i_{b\_\mathrm{fb}} - \frac{K_m}{L_o}\omega_{\mathrm{fb}} \cos(N_r\theta_{\mathrm{fb}}) + \frac{v_{B+} - v_{B-}}{L_o} \tag{3}$$

$$\tau = K_m\left[-i_{a\_\mathrm{fb}} \sin(N_r\theta_{\mathrm{fb}}) + i_{b\_\mathrm{fb}} \cos(N_r\theta_{\mathrm{fb}})\right] - K_{d4} \sin(4N_r\theta_{\mathrm{fb}}) \tag{4}$$

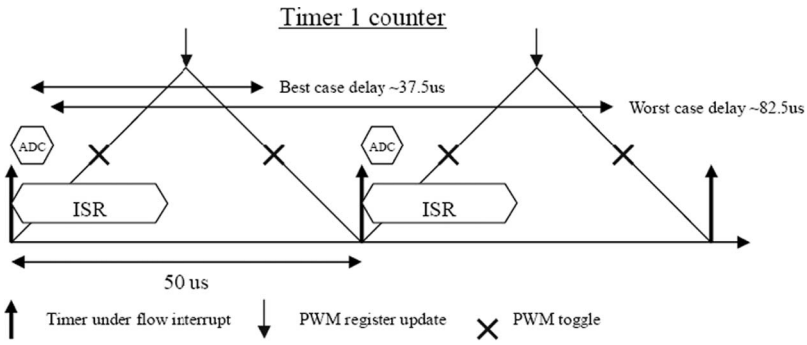

Fig. 3. Interrupt and ISR timing of the DSP controller.

where

- τ torque output (in newton meters);
- K_m force constant (in newton meters per ampere);
- N_r number of pole pairs;
- θ rotor position (in radians);
- K_{d4} amplitude of the fourth-harmonic detent torque (in newton meters).

With microstepping control, the simplified model predicts only one resonant speed, which is caused by the detent torque, the last term in (4). However, this does not match with that of a commercial stepper in real life. For example, the studied motor has three resonant speeds.

The system mentioned earlier is configured to open-loop control, and holding current is set at 1.9 A. The natural frequency of the system calculated by (1) is 142 Hz. On driving the motor with smooth sinusoidal current, three resonant speeds are observed at about 43, 86, and 173 r/min. These correspond to the driving current at 36, 72, and 144 Hz. They are likely to be caused by the detent torque.

At the first resonance (43 r/min/36 Hz), by using (4), it is easy to observe that the frequency of the detent-torque ripple is 36 Hz $\times$ 4 = 144 Hz, which matches with the calculated system natural frequency (142 Hz). Therefore, the first resonance is excited by the fourth-harmonic detent-torque ripple. For the second and third resonances, they occur at doubled speed of the previous resonance. Similarly, there should be first- and second-harmonic detent-torque components which excite the resonances. A torque expression (5) is proposed to describe this characteristic

$$\begin{aligned}\tau = {} & K_m\left[-i_{a\_\mathrm{fb}}\sin(N_r\theta_{\mathrm{fb}}) + i_{b\_\mathrm{fb}}\cos(N_r\theta_{\mathrm{fb}})\right] \\ & - K_{d4}\sin(4N_r\theta_{\mathrm{fb}}) - K_{d2}\sin(2N_r\theta_{\mathrm{fb}} + \phi_2) \\ & - K_{d1}\sin(N_r\theta_{\mathrm{fb}} + \phi_1) - F_s \end{aligned} \tag{5}$$

where

- K_{d1} amplitude of the first-harmonic torque ripple (in newton meters);
- ϕ_1 phase shift of the first-harmonic torque ripple (in radians);
- K_{d2} amplitude of the second-harmonic torque ripple (in newton meters);
- ϕ_2 phase shift of the second-harmonic torque ripple (in radians);
- F_s static friction (in newton meters).

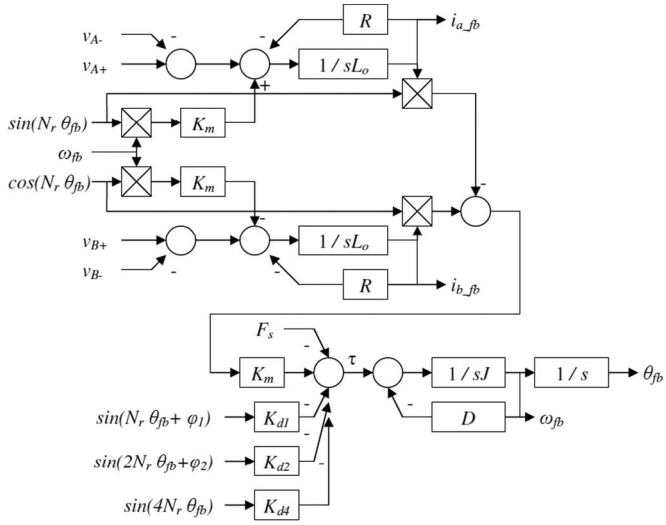

Fig. 4. Block diagram of the proposed stepper model.

Assume that a dummy load is rigidly mounted and that no load torque is applied. The load is described by (6), where D is the damping factor which is assumed to be 0.001 N $\cdot$ m/rad $\cdot$ s^{-1} for a lightly damped system

$$\begin{bmatrix}\dot{\theta}\\ \dot{\omega}\end{bmatrix} = \begin{bmatrix}0 & 1\\ 0 & 0\end{bmatrix}\begin{bmatrix}\theta\\ \omega\end{bmatrix} + \begin{bmatrix}0\\ 1\end{bmatrix}\left[-\frac{D\omega}{J} + \frac{\tau}{J}\right]. \tag{6}$$

The proposed stepper model is shown in Fig. 4, which includes the electric dynamics, torque expression, and a simple inertia load. Note that F_s is the static friction which is a constant value opposing the motion. Since it is a voltage-mode electrical model, simulation frequency needs to be at least 100 kHz for a realistic result.

C. Motor-Characteristic Identification

To fill in the constants K_{d4}, K_{d2}, K_{d1}, ϕ_2, ϕ_1, and F_s in (5), we need to identify the characteristic of the studied stepper motor. The stepper system described in part A is set to run in a modified servo mode with the control algorithm described in (7) and (8). It is a special operation mode for motor-characteristic identification only. The position loop is turned off, and the harmonic torque compensation is turned on. The block diagram of the model of the servo system is shown in Fig. 5 for reference. K_m is set to 0.3, and N_r is set to 50,

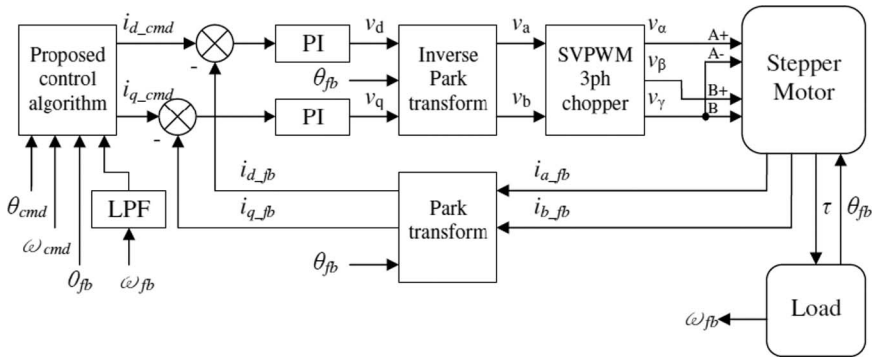

Fig. 5. Block diagram of the servo stepper system.

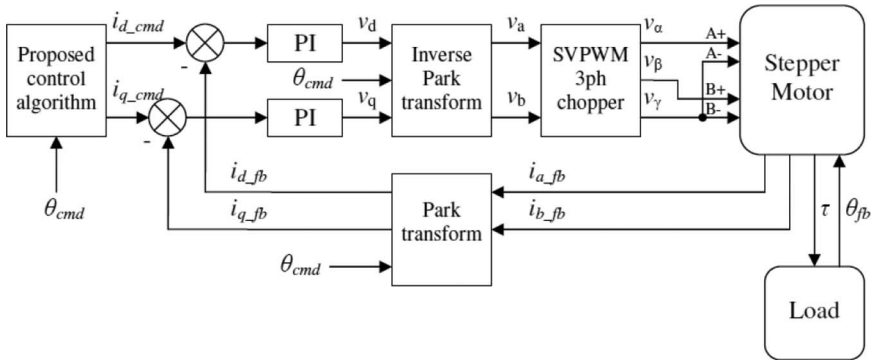

Fig. 6. Block diagram of the open-loop stepper system.

as given by the motor specification. $\theta_{\rm fb}$ is the position feedback obtained from the optical encoder

$$i_{d\_\rm cmd} = 0 \tag{7}$$

$$i_{q\_\rm cmd} = \frac{1}{K_m}\Big[K_{d4}\sin(4N_r\theta_{\rm fb}) + K_{d2}\sin(2N_r\theta_{\rm fb}+\phi_2) + K_{d1}\sin(N_r\theta_{\rm fb}+\phi_1) + F_s\Big]. \tag{8}$$

Current control is done by the digital PI current loop. K_p and K_i are the proportional gain and integration gain of the current loop, respectively,

$$\nu_d = K_p(i_{d\_\rm cmd} - i_{d\_\rm fb}) + K_i\int(i_{d\_\rm cmd} - i_{d\_\rm fb})dt \tag{9}$$

$$\nu_q = K_p(i_{q\_\rm cmd} - i_{q\_\rm fb}) + K_i\int(i_{q\_\rm cmd} - i_{q\_\rm fb})dt. \tag{10}$$

Motor phase currents $i_a i_b$ are transformed to $i_d i_q$ by the well-known Park or DQ transformation [18]

$$\begin{bmatrix} i_{d\_\rm fb} \\ i_{q\_\rm fb}\end{bmatrix} = \begin{bmatrix} \cos(N_r\theta_{\rm fb}) & \sin(N_r\theta_{\rm fb}) \\ -\sin(N_r\theta_{\rm fb}) & \cos(N_r\theta_{\rm fb})\end{bmatrix}\begin{bmatrix} i_{a\_\rm fb} \\ i_{b\_\rm fb}\end{bmatrix}. \tag{11}$$

An external torque is applied to turn the shaft of the motor. The constants to be found are tuned until a minimum resistive torque is observed and a periodic torque ripple is removed. Finally, the motor is like a frictionless dc motor. The results of the identification are $K_{d4} = 0.006$, $K_{d2} = 0.014$, $K_{d1} = 0.011$, $\phi_2 = \pi$, $\phi_1 = \pi/2$, $F_s = 0.029$ (during clockwise motion), and $F_s = -0.029$ (during anticlockwise motion). The unit of all constant K's is newton meters. It is quite unexpected that the first- and second-harmonic torque ripples are much more significant than the fourth-harmonic torque ripple, which is generally thought to be the major component of the detent torque. Significant static friction is observed, which can help a little on damping of motor vibration.

III. Open-Loop Damping Algorithm

A. Damping Algorithm

Based on the proposed torque expression (5) and the identified motor characteristic, the Matlab model of an open-loop system is built, as shown in Fig. 6. The control algorithm (12) and (13) is proposed to damp out the resonances. Flux direction current command $i_{d\_\rm cmd}$, which is equivalent to the amplitude of the excitation current, is set to 1.9 A. Quadrature direction current $i_{q\_\rm cmd}$ is equivalent to torque command when rotor position is equal to position command. It is set to compensate the first-, second-, and fourth-harmonic torque ripples. Constants obtained in the last section are substituted into

$$i_{d\_\rm cmd} = 1.9 \tag{12}$$

$$i_{q\_\rm cmd} = \frac{1}{K_m}\Big[K_{d4}\sin(4N_r\theta_{\rm cmd}) + K_{d2}\sin(2N_r\theta_{\rm cmd}+\phi_2) + K_{d1}\sin(N_r\theta_{\rm cmd}+\phi_1)\Big]. \tag{13}$$

PI current control is described by (9) and (10) in the previous section. For Park transformation, it is basically the same as (11) with position feedback $\theta_{\rm fb}$ replaced by position command $\theta_{\rm cmd}$.

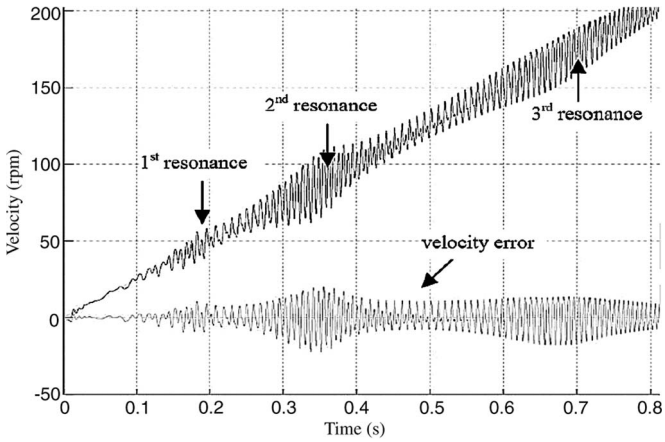

Fig. 7. Simulation result, velocity feedback, and error of the open-loop system without damping.

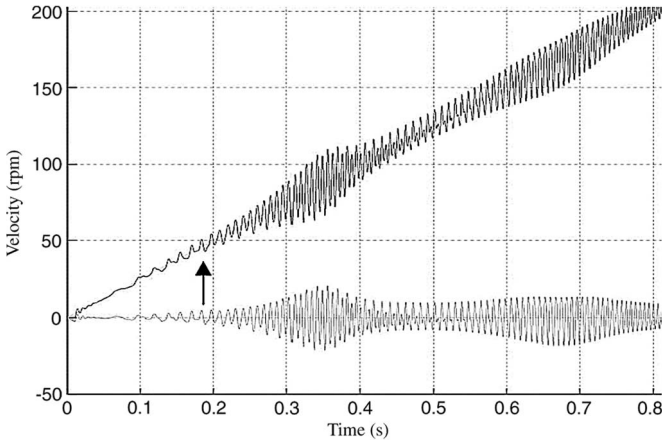

Fig. 8. Simulation result: removal of the first resonance by the injection of the fourth-harmonic torque compensation.

With reference to the work of Yang *et al.* [19], the three-phase space-vector (SV) PWM driving scheme is described by

$$\begin{bmatrix} v_\alpha \\ v_\beta \\ v_\gamma \end{bmatrix} = \begin{bmatrix} 1 & 0 & 1 \\ 0 & 1 & 1 \\ 0 & 0 & 1 \end{bmatrix} \begin{bmatrix} v_a \\ v_b \\ v_o \end{bmatrix} \tag{14}$$

$$v_{\max} = Maximum\{v_a, v_b, 0\} \tag{15}$$

$$v_{\min} = Minimum\{v_a, v_b, 0\} \tag{16}$$

$$v_o = \frac{v_i}{2} - \frac{(v_{\max} + v_{\min})}{2} \tag{17}$$

where v_i is the bus voltage supply of the SVPWM chopper.

To simulate the characteristic of the periodic PWM update of the chopper drive, the zero-order hold is applied on $v_\alpha v_\beta v_\gamma$.

B. Simulation Results

In all simulations, the command is a speed ramp from 0 r/min at $t = 0$ s to 200 r/min at $t = 0.8$ s. In the first case (Fig. 7), no damping is applied, so $i_{q\_\mathrm{cmd}} = 0$. Three resonant speeds are observed at about 45, 80, and 170 r/min which match with 43, 86, and 173 r/min observed in the experiment, respectively.

With the injection of the fourth-harmonic torque compensation, the first resonance is damped out (Fig. 8). Similarly, the injection of the first- and second-harmonic torque compensations can damp out the second and third resonances, respectively (Figs. 9 and 10). The amplitude of velocity error is most significant at the second resonance, which is caused by the relatively large second-harmonic detent-torque ripple. Fig. 11 shows the results of the injection of all the three harmonic torque compensations in i_{q_cmd}. The velocity ripple is almost eliminated in the whole low-speed range.

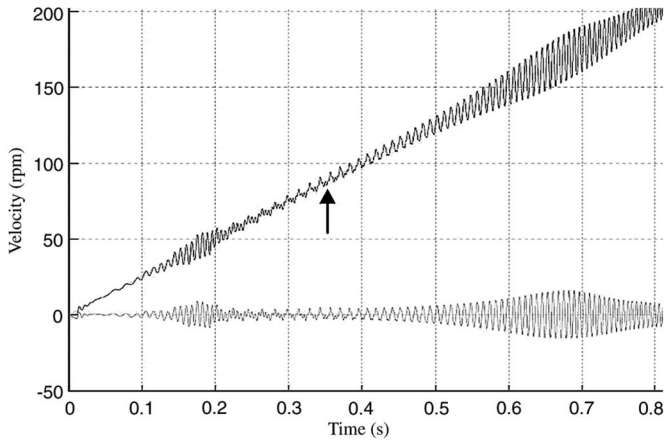

Fig. 9. Simulation result: removal of the second resonance by the injection of the second-harmonic torque compensation.

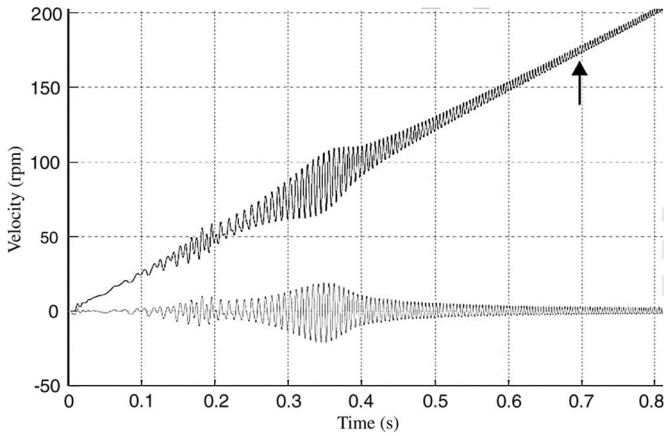

Fig. 10. Simulation result: removal of the third resonance by the injection of the first-harmonic torque compensation.

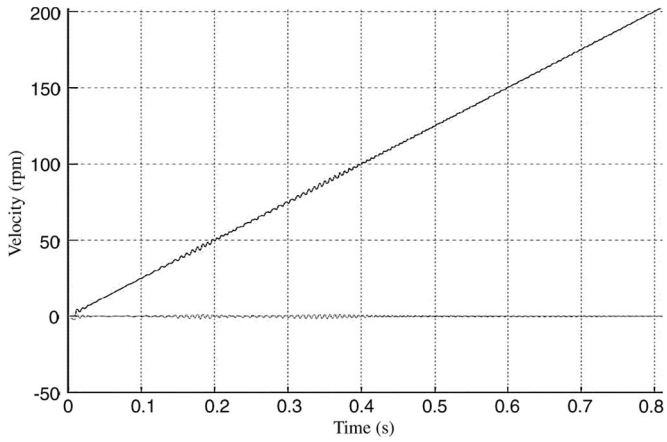

Fig. 11. Simulation result: removal of all three resonances by the injection of the first-, second-, and fourth-harmonic torque compensations.

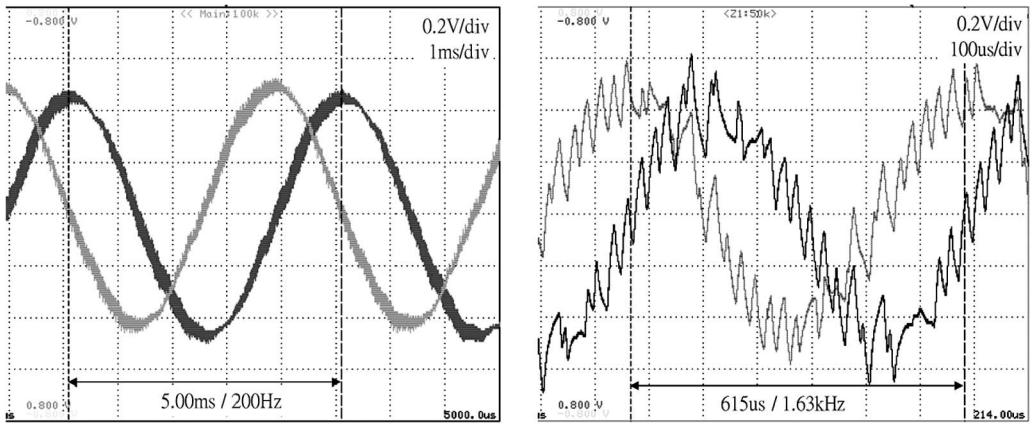

Fig. 12. Experimental result: motor phase current waveform at (left) 200 Hz and (right) 1.6 kHz. Current sensor: 2.5 A/V.

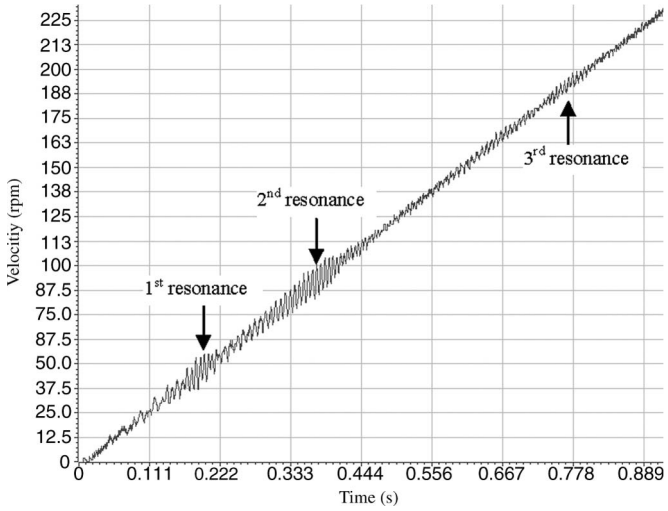

Fig. 13. Experimental result: velocity feedback without damping.

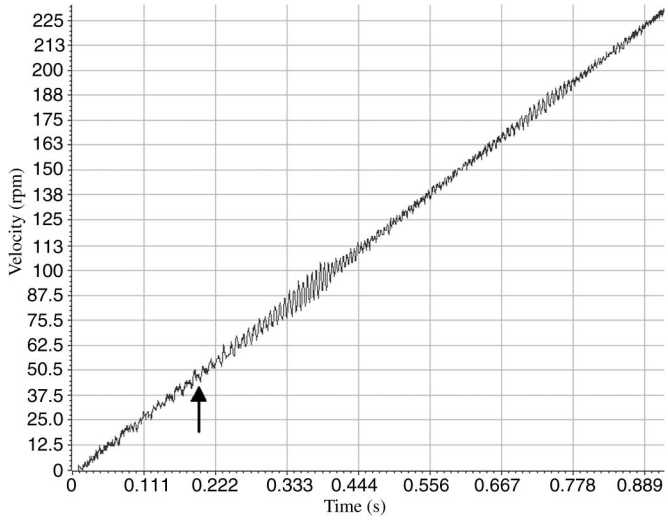

Fig. 14. Experimental result: removal of the first resonance by the injection of the fourth-harmonic torque compensation.

Note that, at all three resonances, the frequency of velocity error is the same which corresponds to the natural frequency f_n of the system (calculated to be 144 Hz). Moreover, if the load torque is applied, the damping performance is expected to be degraded. It is because the equilibrium position of the rotor will shift to a certain degree from the original position. Fine tuning of ϕ_1 and ϕ_2 will be needed to offset the change.

C. Experimental Results

The proposed damping and control algorithm is coded into the DSP controller. The current loop is tuned ($K_p = 7.5$ and $K_i = 0.01$) to ensure good current tracking even when the motor is running at high speed. The current loop is therefore transparent to the control algorithm. Fig. 12 shows that there is no waveform distortion, phase distortion, and amplitude falloff at 1.6-kHz (1920 r/min) motor phase current waveform, as compared with that at 200 Hz (240 r/min). The chopping ripple is significant due to the high back electromotive force (estimated to be about 60 V at 1920 r/min) at that speed. The waveform is, in fact, the current feedback from Hall-effect current sensors. Any offset voltage is calibrated in the DSP controller.

The motor is set to run a speed ramp from 0 r/min at $t = 0$ s to 250 r/min at $t = 1$ s, which is similar to that in simulation. The DSP is programmed to data log the velocity feedback at 2-kHz sampling rate. The system is first set to run without damping. It is then tested with the injection of the fourth-, second-, and first-harmonic torque compensations to damp out the first, second, and third resonances, respectively. Finally, it is tested with the injection of all the three harmonic torque compensations. The results are shown in Figs. 13–17, respectively, which can be directly compared with the corresponding simulation results shown in Figs. 7–11. Experimental results show a close match with simulation results. The proposed algorithm can damp out vibration and resonances effectively.

Further experiment is done to investigate constant-speed operation at resonant speed. Velocity error, which is calculated by subtracting feedback velocity from setpoint velocity, is data logged at 20 kHz. The motor is set to run at constant speed at the first (43 r/min), second (86 r/min), and third (173 r/min) resonant speeds to observe the effect of the proposed damping algorithm. The first resonance is damped out by the injection of the fourth-harmonic torque compensation (Fig. 18). The second resonance is damped out by the injection of the second-harmonic torque compensation (Fig. 19). The third resonance

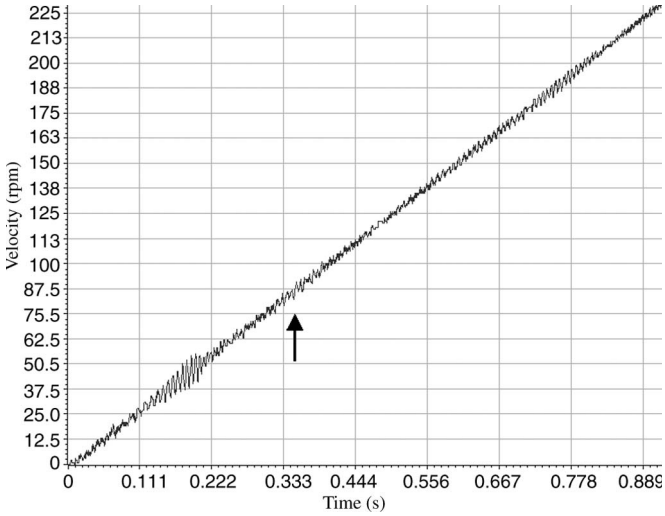

Fig. 15. Experimental result: removal of the second resonance by the injection of the second-harmonic torque compensation.

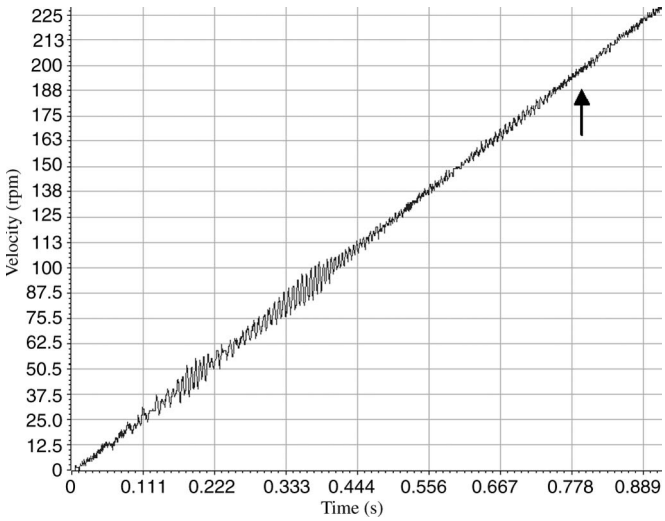

Fig. 16. Experimental result: removal of the third resonance by the injection of the first-harmonic torque compensation.

is damped out by the injection of the first-harmonic torque compensation (Fig. 20). A high-frequency ripple is observed in the experimental result, which is caused by the differentiation of the finite-resolution position feedback in the quadrature-encoder-pulse-based velocity measurement.

The frequency of velocity error is the same in all three resonances which matched the simulation results. This means that they are caused by the same mechanical natural frequency. However, they are triggered by the torque ripple of the three different harmonics. Resonance occurs when the frequency of any one of the torque ripple harmonics matches the natural frequency.

IV. Servo-Mode Damping Algorithm

A. Damping Algorithm

The Matlab model of a servo controlled stepper system is built, as shown in Fig. 5. The damping and control algorithm (18) and (19) is proposed. Flux direction current command

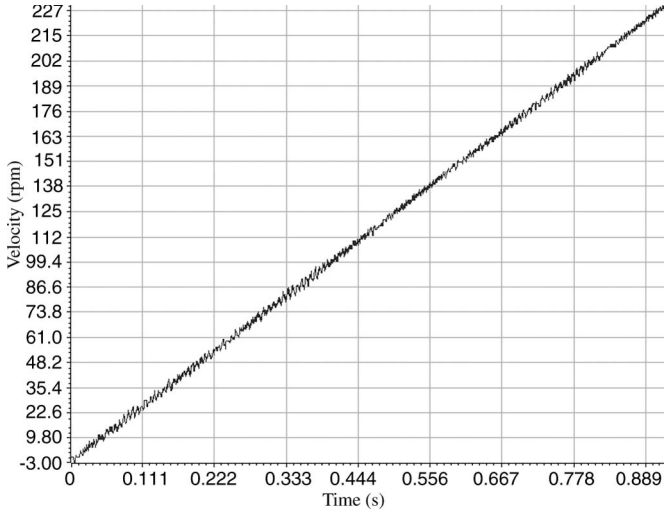

Fig. 17. Experimental result: removal of all three resonances by the injection of the first-, second-, and fourth-harmonic torque compensations.

i_{d_cmd} is set to zero. Quadrature direction current i_{q_cmd}, which is equivalent to torque command, contains position PID control and harmonic torque ripple compensation. The first three terms are differentiation, proportion, and integration control of position error, respectively. K_{p_vel}, K_{p_pos}, and K_{i_pos} are the control parameters of the standard position PID loop. The four terms afterward are the torque ripple compensations at the fourth, second, first harmonics and the static friction compensation. The proposed controller is shown in Fig. 21

$$i_{d\_\mathrm{cmd}} = 0 \tag{18}$$

$$i_{q\_\mathrm{cmd}} = \frac{1}{K_m}\Big[K_{p\_\mathrm{vel}}\omega_{\mathrm{err}} + K_{p\_\mathrm{pos}}\theta_{\mathrm{err}} + K_{i\_\mathrm{pos}}\int \theta_{\mathrm{err}}dt + K_{d4}\sin(4N_r\theta_{\mathrm{fb}}) + K_{d2}\sin(2N_r\theta_{\mathrm{fb}} + \phi_2) + K_{d1}\sin(N_r\theta_{\mathrm{fb}} + \phi_1) + F_s\Big] \tag{19}$$

where $\omega_{\mathrm{err}} = \omega_{\mathrm{cmd}} - \omega_{\mathrm{fb}}$ and $\theta_{\mathrm{err}} = \theta_{\mathrm{cmd}} - \theta_{\mathrm{fb}}$.

B. Simulation Results

The simulated velocity feedback and error of the system are shown in Figs. 22 and 23. In both simulations, the command is a speed ramp from 0 r/min at $t = 0$ s to 100 r/min at $t = 1$ s. In the first case (Fig. 22), no damping is applied. The control law contains position PID control only. The smoothness of the motion is unsatisfactory. Fig. 23 shows the results with the injection of the torque compensation components in i_{q_cmd}, as described in (19). The smoothness of the motion is significantly improved.

Some high-frequency ripple is observed before $t = 0.1$ s. This is caused by the quantization noise of the encoder position feedback which results in noise in the position loop. It can be removed immediately if we assume a higher encoder resolution, for example, 40 000 pulses/rev. However, such a system would be too expensive to be commercially feasible.

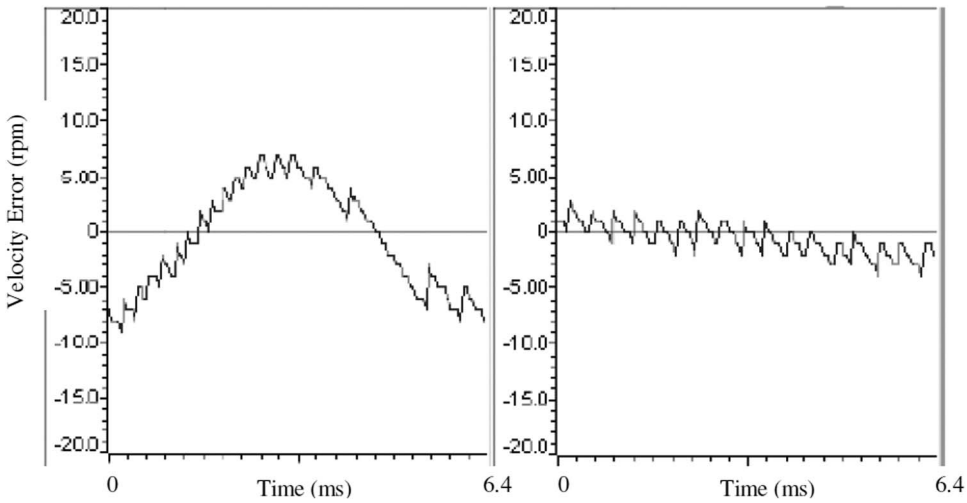

Fig. 18. Experimental result: velocity error at 43 r/min (left) without damping and (right) with damping.

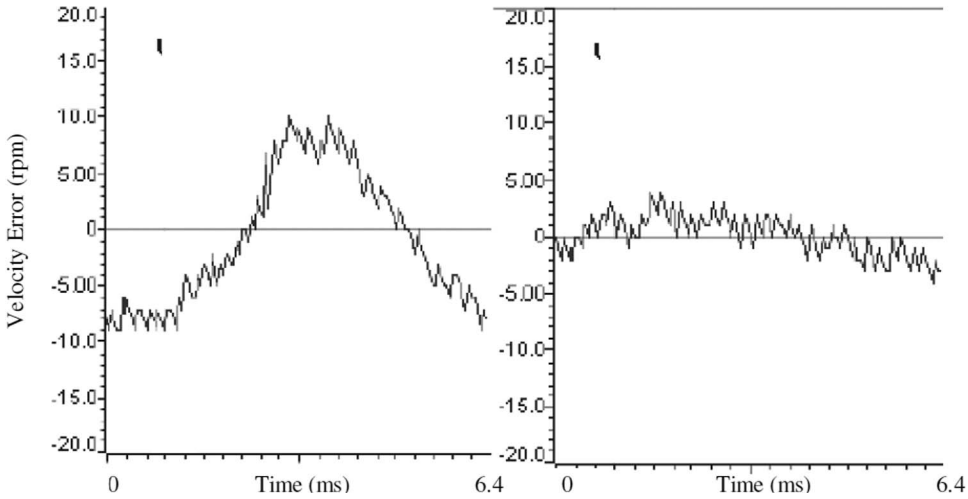

Fig. 19. Experimental result: velocity error at 86 r/min (left) without damping and (right) with damping.

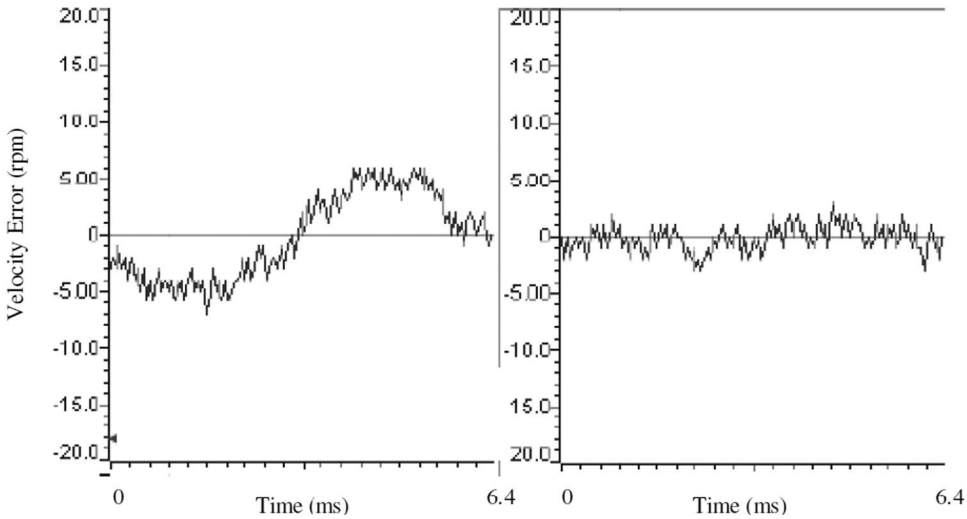

Fig. 20. Experimental result: velocity error at 173 r/min (left) without damping and (right) with damping.

The effect of the finite resolution of the encoder is modeled by quantization of $\theta_{\rm fb}$. For our system, the encoder resolution is 4000 pulses/rev. This means that the position resolution is only 20 counts/step with our 200-step/rev stepper motor. It is expected to limit the accuracy of position control and current control.

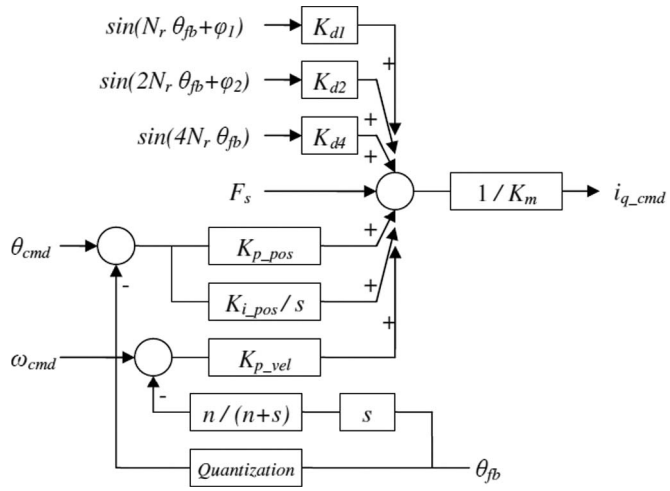

Fig. 21. Model of the proposed servo controller.

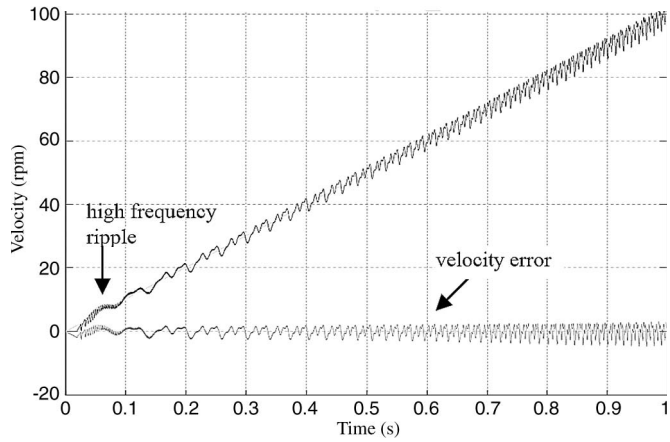

Fig. 22. Simulated velocity feedback and error of the servo system without damping.

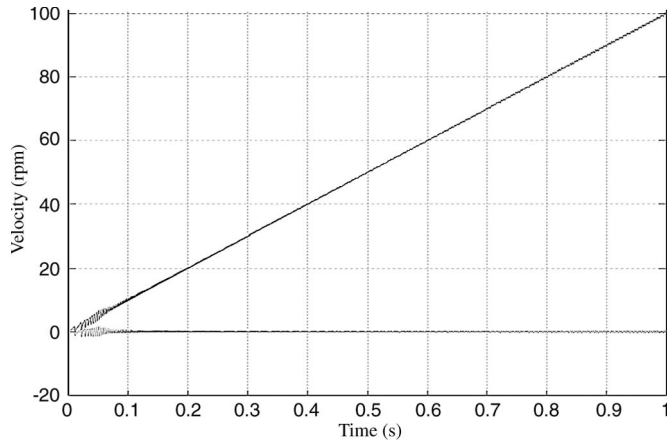

Fig. 23. Simulated velocity feedback and error of the servo system with the proposed damping algorithm.

C. Experimental Results

The proposed control and damping algorithm is coded into the DSP controller. The position-loop update rate is set to 4 kHz which is enough for typical industrial applications. The position loop is tuned ($K_{p\_\mathrm{pos}} = 0.1$, $K_{i\_\mathrm{pos}} = 0.01$, and $K_{p\_\mathrm{vel}} = 0.3$) so that it is stable over a wide velocity range (0–1200 r/min).

The experiment is done to verify the damping performance. The system is first set running without damping. K_{d1}, K_{d2}, K_{d3}, and F_s of (19) are therefore set to zero. The system is set to ramp from 0 to 100 r/min in 1 s. Significant vibration is observed, particularly when the motor speed is below 50 r/min. Then, the proposed damping algorithm is applied, and the system is set to run the same speed ramp again. Motor vibration is significantly reduced. Unlike that in open-loop mode, no resonance is observed in servo mode. It is because there is no holding torque and equilibrium position. The system does not therefore have natural frequency. The frequency of vibration increases with motor velocity, as shown in the simulation results.

As velocity feedback is calculated by differentiating position feedback, the resolution of the velocity depends on the sample rate as well as the resolution of the encoder [20]. In our system, the calculation is done at 20 kHz. This means that the resolution of the velocity feedback is $1/4000 \times 20\,000 \times 60 = 300$ r/min. A low-pass filter (LPF) is needed to suppress the quantization noise. However, the LPF makes the system less responsive to velocity error. In our experiment, the LPF is implemented by a first-order digital infinite impulse response at 32-Hz bandwidth.

V. Conclusion

The characteristic of a commercial hybrid stepper motor is successfully modeled by the proposed torque expression. It is quite unexpected that the first- and second-harmonic torque ripples contribute significantly to low-speed resonance, while the effect of the higher order harmonics is relatively weak. Model-based compensation of the low-order torque ripple is proven to be effective to remove vibration and resonance. Simulation and experimental results show that the proposed damping algorithms work in both open-loop and servo modes. The algorithms are efficient enough to be used in demanding application with commercial DSP-based hardware platform.

More works will follow on the application of the damping algorithm. Also, the parameter sensitivity of the algorithm needs to be studied.

A patent is pending on the methodology/hardware setup presented in this paper (application S/N: 60/866, 638 filed on November 21, 2006).

Acknowledgment

The authors would like to thank S. W. Tam and Dr. W. C. Gan for their helpful suggestions.

References

[1] T. Kanjo and A. Sugawara, *Stepping Motors and Their Microprocessor Controls*. Oxford, U.K.: Clarendon, 1994.
[2] P. Acarnley, *Stepping Motors: A Guide to Theory and Practice*, 4th ed. Stevenage, U.K.: Inst. Elect. Eng., 2002.
[3] R. H. Brown and K. Srinivas, "A damping circuit for chopper driven bifilar hybrid step motors," in *Proc. IEEE Power Electron. Spec. Conf.*, 1989, vol. 1, pp. 446–451.
[4] S. Schweid, J. Mcinroy, and R. Lofthus, "Closed loop low-velocity regulation of hybrid stepping motors amidst torque disturbance," *IEEE Trans. Ind. Electron.*, vol. 42, no. 3, pp. 316–324, Jun. 1995.

[5] M. Zribi and J. Chiasson, "Position control of a PM stepper motor by exact linearization," *IEEE Trans. Autom. Control*, vol. 36, no. 5, pp. 620–625, May 1991.
[6] P. Crnosija, B. Kuzmanovic, and S. Ajdukovic, "Microcomputer implementation of optimal algorithms for closed-loop control of hybrid stepper motor drives," *IEEE Trans. Ind. Electron.*, vol. 47, no. 6, pp. 1319–1325, Dec. 2000.
[7] W. D. Chen, K. L. Yung, and K. W. Cheng, "Profile tracking performance of a low ripple hybrid stepping motor servo drive," *Proc. Inst. Elect. Eng.—Control Theory Appl.*, vol. 150, no. 1, pp. 69–76, Jan. 2003.
[8] W. D. Chen, K. L. Yung, and K. W. Cheng, "A learning scheme for low-speed precision tracking control of hybrid stepping motors," *IEEE/ASME Trans. Mechatronics*, vol. 11, no. 3, pp. 362–365, Jun. 2006.
[9] F. Betin, D. Pinchon, and G.-A. Gapolino, "Fuzzy logic applied to speed control of a stepping motor drive," *IEEE Trans. Ind. Electron.*, vol. 47, no. 3, pp. 610–622, Dec. 2000.
[10] T.-S. Hwang, J.-K. Seok, and D.-H. Kim, "Active damping control of linear hybrid stepping motor for cogging force compensation," *IEEE Trans. Magn.*, vol. 42, no. 2, pt. 2, pp. 329–334, Feb. 2006.
[11] S. Goodnick, "Electronic damping cures step motor resonance—Part II: Damping technique," *Power Conv. Intell. Motion*, vol. 23, no. 5, pp. 32–43, May 1997.
[12] S.-M. Yang and E.-L. Kuo, "Damping a hybrid stepping motor with estimated position and velocity," *IEEE Trans. Power Electron.*, vol. 18, no. 3, pp. 880–887, May 2003.
[13] B. K. Bose, "Neural network applications in power electronics and motor drives—An introduction and perspective," *IEEE Trans. Ind. Electron.*, vol. 54, no. 1, pp. 14–33, Feb. 2007.
[14] E. N. Sanchez, A. G. Loukianov, and R. A. Felix, "Dynamic triangular neural controller for stepper motor trajectory tracking," *IEEE Trans. Syst., Man, Cybern. C, Appl. Rev.*, vol. 32, no. 1, pp. 24–30, Feb. 2002.
[15] A. Rubaai and R. Kotaru, "Adaptation learning control scheme for a high-performance permanent-magnet stepper motor using online random training of neural networks," *IEEE Trans. Ind. Appl.*, vol. 37, no. 2, pp. 495–502, Mar./Apr. 2001.
[16] A. Rubaai and M. Castro, "Experiment implementation of an adaptive neural network tracking controller for motion control of step motors," in *Conf. Rec. 40th IEEE IAS Annu. Meeting*, Oct. 2005, vol. 1, pp. 693–699.
[17] A. Rubaai, M. J. Castro-Sitiriche, M. Garuba, and L. Burge, "Implementation of artificial neural network-based tracking controller for high-performance stepper motor drives," *IEEE Trans. Ind. Electron.*, vol. 54, no. 1, pp. 218–227, Feb. 2007.
[18] F. Khorrami, P. Krishnamurthy, and H. Melkote, *Modeling and Adaptive Nonlinear Control of Electric Motors*. New York: Springer-Verlag, 2003.
[19] S.-M. Yang, F.-C. Lin, and M.-T. Chen, "Micro-stepping control of a two-phase linear stepping motor with three-phase VSI inverter for high-speed applications," *IEEE Trans. Ind. Appl.*, vol. 40, no. 5, pp. 1257–1264, Sep./Oct. 2004.
[20] M. Bodson, J. N. Chiasson, R. T. Novotnak, and R. B. Rekowski, "High-performance nonlinear feedback control of a permanent magnet stepper motor," *IEEE Trans. Control Syst. Technol.*, vol. 1, no. 1, pp. 5–14, Mar. 1993.

Kenneth Wang-Hay Tsui was born in Hong Kong in 1982. He received the B.Eng. degree in electronic and communication engineering from The University of Hong Kong, Hong Kong, in 2004. He is currently working toward the M.Phil. degree at The Hong Kong Polytechnic University, Kowloon, Hong Kong.

Since 2004, he has been an Electronic Engineer with ASM Assembly Automation Ltd., Hong Kong. His research interests include motor control, high-performance motor drives, and industrial applications.

Norbert Chow Cheung (S'85–M'91–SM'05) received the B.Sc. degree from the University of London, London, U.K., in 1981, the M.Sc. degree from The University of Hong Kong, Hong Kong, in 1987, and the Ph.D. degree from the University of New South Wales, Kensington, Australia, in 1996.

He worked for two years as a Technical Manager with ASM Assembly Automation Ltd., Hong Kong, in the areas of intelligent motion control and robotics systems. He has been with The Hong Kong Polytechnic University, Kowloon, Hong Kong, since 1997, where he is currently with the Department of Electrical Engineering.

Dr. Cheung is a Chartered Engineer in the U.K. and a member of the Institution of Engineering and Technology, U.K.

Kadett Chi-Wah Yuen received the B.S. degree from the City Polytechnic of Hong Kong (currently City University of Hong Kong), Kowloon, Hong Kong, in 1989.

He is currently a Principal Engineer with ASM Assembly Automation Ltd., Hong Kong. His main area of interest is machinery electronic systems.